Orthodontics & Craniofacial Research

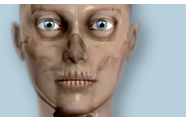

ORIGINAL ARTICLE

Y.-M. Yang
J. Lee
Y.-I. Kim
B.-H. Cho
S.-B. Park

Axial cervical vertebrae-based multivariate regression model for the estimation of skeletal-maturation status

Authors' affiliations:
Y.-M. Yang, J. Lee, Y.-I. Kim, S.-B. Park, Department of Orthodontics, School of Dentistry, Dental Research Institute, Pusan National University, Yangsan, South Korea
Y.-I. Kim, Biomedical Research Institute, Pusan National University Hospital, Busan, South Korea
B.-H. Cho, Department of Oral & Maxillofacial Radiology, School of Dentistry, Pusan National University, Yangsan, South Korea

Correspondence to:
Dr Y.-I. Kim
Biomedical Research Institute
Pusan National University Hospital
Gudeokro 305, Seogu
Busan 602-739, South Korea
E-mail: kimyongil@pusan.ac.kr

Date:
Accepted 21 March 2014

DOI: 10.1111/ocr.12045

Yang Y.-M., Lee J., Kim Y.-I., Cho B.-H., Park S.-B. Axial cervical vertebrae-based multivariate regression model for the estimation of skeletal-maturation status
Orthod Craniofac Res 2014; **17**:187–196. © 2014 John Wiley & Sons A/S. Published by John Wiley & Sons Ltd

Structured Abstract

Objectives – This study aimed to determine the viability of using axial cervical vertebrae (ACV) as biological indicators of skeletal maturation and to build models that estimate ossification level with improved explanatory power over models based only on chronological age.

Materials and Methods – The study population comprised 74 female and 47 male patients with available hand-wrist radiographs and cone-beam computed tomography images. Generalized Procrustes analysis was used to analyze the shape, size, and form of the ACV regions of interest. The variabilities of these factors were analyzed by principal component analysis. Skeletal maturation was then estimated using a multiple regression model.

Results – Separate models were developed for male and female participants. For the female estimation model, the adjusted R^2 explained 84.8% of the variability of the Sempé maturation level (SML), representing a 7.9% increase in SML explanatory power over that using chronological age alone (76.9%). For the male estimation model, the adjusted R^2 was over 90%, representing a 1.7% increase relative to the reference model.

Conclusions – The simplest possible ACV morphometric information provided a statistically significant explanation of the portion of skeletal-maturation variability not dependent on chronological age. These results verify that ACV is a strong biological indicator of ossification status.

Key words: axial cervical vertebra maturation; geometric morphometrics; principal component analysis; Procrustes analysis; Sempé maturation level

Introduction

The assessment of craniofacial growth and development is a crucial component of orthodontic diagnosis, especially when

considering growth modification and orthognathic surgery as treatment options. For this reason, many researchers have sought valid identifiers of somatic ossification status to support the assessment of mandibular skeletal-maturation level. Previously determined identifiers include chronological age, dental development, sexual maturation, voice change, and body height, and these identifiers have been used to develop many maturation indices for determining treatment timing (1–4).

Unfortunately, while it is of the utmost clinical convenience, chronological age alone is not a reliable indicator of skeletal maturation. Among other maturation indices, cervical vertebral maturation (CVM) methods based on lateral cephalometric films—such as those developed by Todd and Pyle, Lamparski, and Hassel and Farman (5–7)—have proved effective for assessing adolescent growth peaks of both body height and mandibular size (8, 9). O'Reilly and Yanniello (2) evaluated the relationship between CVM and mandibular growth changes, and Franchi et al. (8) confirmed the validity of six CVM stages as biological indicators of both somatic and mandibular skeletal maturation. However, Gabriel et al. (10) raised concerns about the poor reproducibility of CVM methods, noting that the interobserver agreement was below 50% and the intraobserver agreement was only slightly better at 62%.

To improve CVM analysis and make it applicable to more patients, Chen et al. (11) used fewer vertebral bodies and more sensitive staging parameters for quantitative CVM assessment. To examine CVM in a more quantitative and statistical-analytical regard, Chatzigianni and Halazonetis (12) applied geometric morphometric analysis to the evaluation of cervical vertebrae shape. Statistical shape analysis involves the geometric analysis of a set of shapes, through which relevant statistics are measured to identify similar geometric properties among different groups. Important uses of shape analysis include determination of distance between shapes, estimation of average shapes from samples, and estimation of shape variability among samples (13). While these previous CVM studies have used the lateral aspect, in the present study we investigated CVM from the axial aspect, examining the cervical vertebral structure. To this end, we applied cone-beam computed tomography (CBCT), which is a useful tool for investigating axial cervical vertebrae (ACV) structure (14, 15). We also utilized three-dimensional image analysis software programs, which are useful shape-analysis tools for extracting landmark coordinates in a region of interest (ROI). To quantitate growth status validated from hand-wrist radiographs, we used the Sempé maturation level (SML; 16), which we found to be highly correlated with Fishman's skeletal-maturation index (FMI).

With these tools, here we investigated the viability of using axial cervical vertebrae maturation (ACVM) as a biological indicator of skeletal maturation. We further aimed to simultaneously build a model that best estimated ossification level, with improved explanatory power over that of a model based only on chronological age. The ultimate goal of this study was to find statistically significant ROIs in ACV shapes, which would improve prediction models using hand-wrist radiographs when utilized in addition to the reference chronological-age-based simple linear model.

Materials and methods

The sample population comprised 74 female and 47 male patients who were 6–18 years of age and had available hand-wrist radiographs (PM2002CC; Plameca, Helsinki, Finland) and CBCT images (Pax-zenith3D; Vatech, Seoul, Korea). Exclusion criteria were cleft lip and/or palate, trauma, or syndromes (Table 1). This study was reviewed and approved by the Institutional Review Board of Pusan National University Hospital (E-2011008).

All hand-wrist radiographs were evaluated by a single investigator to determine the SML and FMI (38). The FMI is more widely used by clinicians, and statistical analysis was performed to confirm the correspondence between FMI and SML. CBCT data were acquired on the same date

Table 1. **Descriptive statistics of subjects**

Sample size (gender/number)	Female/74	Male/47
Chronological age		
Mean	14.6	14.0
Max	18.0	18.0
75% quartile	16.6	16.5
Median	15.3	15.1
25% quartile	13.6	12.1
Min	5.5	5.9
Sempé maturation level (SML)		
Mean	830.6	712.7
Max	948.0	928.0
75% quartile	909.0	894.0
Median	879.5	850.0
25% quartile	827.5	641.0
Min	202.0	131.0
Fishman's skeletal-maturation index (FMI)		
Mean	9.4	7.4
Max	11	11
75% quartile	11	11
Median	11	10
25% quartile	10	4
Min	1	1

as the hand-wrist radiographs. CBCT was performed with the subject in an upright position for maximum intercuspation. The FH plane was set parallel to the floor. The CBCT scanning settings were as follows: field of view, 20 × 19 cm; tube voltage, 90 kVp; tube current, 4.0 mA; and scan time, 24 s. The CBCT data were reconstructed with 3D imaging software (OnDemand3D; Cybermed Co., Seoul, Korea). CBCT data were used for axial CT image acquisition of ACV shapes. ACV images were obtained using 3D image software with a window width of 4000 and window level of 1000.

Axial CT image acquisition protocol

We designed and tested an ACV image scanning protocol for reproducible acquisition. This protocol used the atlas (C1) of each subject as a basis and axis for axial image scanning (Fig. 1). Maintaining the vertical axis, a band of image layers was chosen for each cervical vertebra in the sagittal view. For maximally distinguishable image acquisition, C1 and the axis (C2) were assumed to share the same vertical axis, and the third (C3) and fourth (C4) cervical vertebrae were assumed to share another axis. The procedure was as follows (Fig. 2):

1. C1: A band of axial image layers was chosen to maximize the band width within the posterior arch, with neither the upper nor the lower border of the band trespassing on either the upper or lower cortical lamina in the sagittal view;
2. C2: A band was chosen to encompass the whole vertical span of the posterior arch;
3. In sagittal view, the origin was relocated to the lowermost point of the posterior lamina of the C4 body, followed by adjustment of the vertical axis so as to pass through the uppermost point of the posterior lamina of the C3 body farthest from the new origin;
4. C3 and C4: A band of axial image layers was chosen within each C3 and C4 body, with the width of each maximized so as to not trespass on the lower border of the cortical lamina of the body but to encompass the whole anterior curvature of the corresponding body.

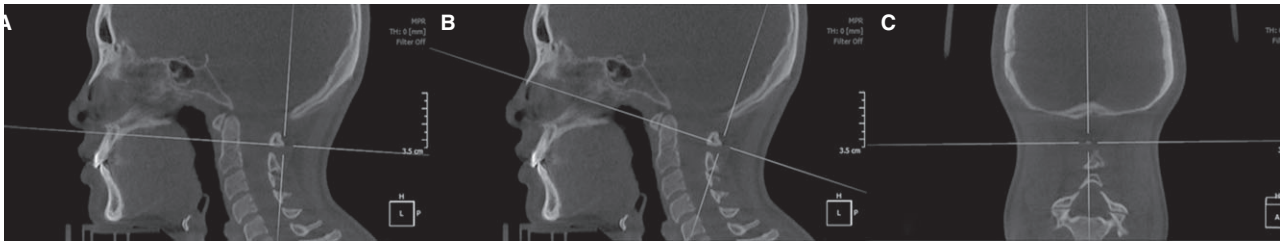

Fig. 1. Axial CT image acquisition protocol: setting of C1 origin. (A) Axes origin located at the most posterior point of the atlas (C1) in sagittal view. (B) Most anterior and posterior points of C1 used as the anterior–posterior axis in axial view. (C) Vertical axis adjusted to pass through the foramen magnum midpoint in coronal view.

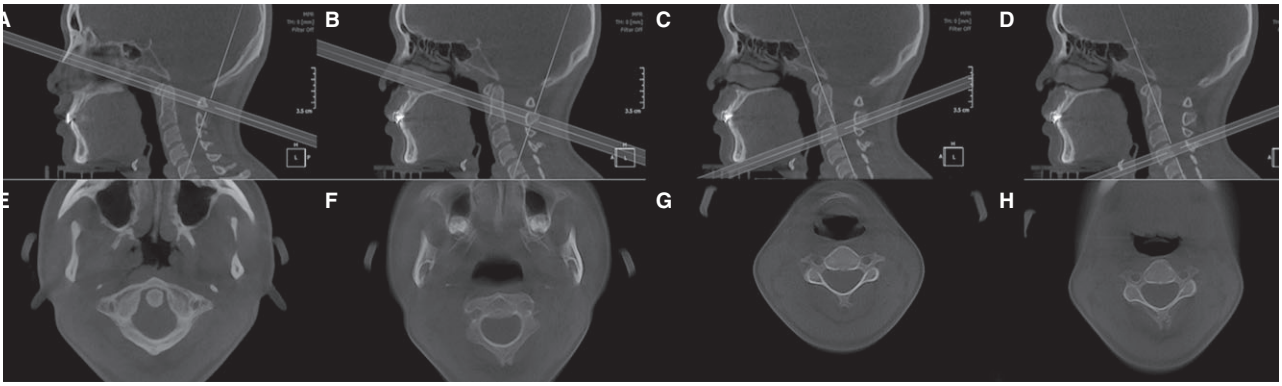

Fig. 2. Axial CT image acquisition protocol: chosen bands of C1–C4 axial image layers and axial cervical vertebrae (ACV) images. (A, E) Band of C1 axial image layer and obtained maximum intensity projection (MIP) ACV image. (B, F) Band of C2 axial image layer and obtained multiplanar reformation (MPR) ACV image. (C, G) Band of C3 axial image layer and obtained MPR ACV image. (D, H) Band of C4 axial image layer and obtained MPR ACV image.

When a band was chosen for the corresponding cervical vertebrae, an axial image was acquired in the axial view. For improved distinguishability, maximum intensity projection (MIP) images were acquired and used for C1 shape analysis, as were multiplanar reformation (MPR) images for other vertebrae.

Generalized Procrustes analysis and principal component analysis

In preparation for Generalized Procrustes analysis (GPA), a set of landmarks was placed in each ACV to generate potential ROIs. The landmarks were chosen and subjected to coordinate extraction. The landmarks composing each ROI for ACV1 to ACV4 are shown and defined in Fig. 3 and Table 2. Axial cervical vertebrae landmark identification for each subject was performed by a single investigator, after which each landmark was electronically marked and its corresponding x–y coordinates were extracted using DentPhotoCeph (Akerrmedia, Iksan, South Korea). Statistical computation was performed using the language R (Vienna, Austria), a widely used statistical program and open-source software.

For each subject, a full GPA was performed to analyze the shapes and sizes of the ACV ROIs, and a partial GPA was applied to analyze the forms (13, 17). Immediately thereafter, a principal component analysis (PCA) was performed to analyze the variabilities of these factors among the subjects (13). The PCA yielded two PC1 scores for each ROI, in both shape space and form space, with centroid size as the size factor. The shape and form PC1 scores summarized the largest percentages of shape and form variability, respectively, with the dimensions of such spaces greatly reduced to 1 if only the first PC score was used.

The meaningful ROIs of each ACV were selected using multiple regression models to test their viability as biological predictors of skeletal-maturation level that improved the SML explanatory power of the simple chronological-age-based regression model. In the final stage of analysis, multiple regression models based on such viable biological predictors were assessed

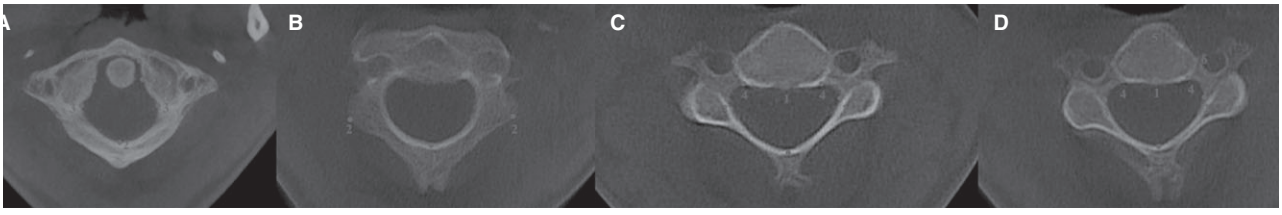

Fig. 3. Model regions of interest (mROIs) for each axial cervical vertebra (ACV) and their landmarks: atlas, C1 (A); axis, C2 (B); third cervical vertebra, C3 (C); fourth cervical vertebra, C4 (D).

Table 2. **Landmark defined from model region of interest (mROI)**

	mROI	Landmarks	Number in Fig. 3
1st Axial cervical vertebra	Vertebral foramen	Most anterior point	(1)
		Most posterior point	(2)
		Most distant point, right and left	(3) Rt. and Lt
		Deepest point from odontoid process located anteriorly to anterior 1/2 of odontoid process and where curvature of articular surface begins, right and left	(4) Rt. and Lt.
		Farthest point away from line joining (3) and (4) and located between (3) and (4), right and left	(5) Rt. and Lt.
2nd Axial cervical vertebra	Posterior arch triangle	Most posterior point in vertebral foramen	(1)
		Most distant point of the vertebral arch, right and left	(2) Rt. and Lt.
3rd and 4th axial cervical vertebrae (ACV3, ACV4)	Vertebral foramen	Most posterior point of vertebral body	(1)
		Most posterior point of vertebral foramen	(2)
		Most distant point of vertebral foramen, right and left	(3) Rt. and Lt.
		Deepest possible point of anterior part of vertebral foramen from line joining (1) and (3) located on posterior lamina of vertebral body, right and left	(4) Rt. and Lt.
	Vertebral body	Most anterior point of vertebral body	(5)
		Most distant point of vertebral body, right and left	(6) Rt. and Lt.
		Most posterior point of vertebral body	(1)
		Same points as in ACV4 (4), right and left	(4) Rt. and Lt.

in terms of the statistical significance of their estimates. Those models that attained the most acceptable statistical significance of model structure and estimates were selected, with different models chosen for the female and male subpopulations.

Results

Pearson's correlation coefficients were used to demonstrate the correspondence between the SML and FMI. For the female and male patients, these values were 0.950 and 0.956, respectively, suggesting a potentially strong commutability of SML and FMI results. Shapiro–Wilk testing confirmed normal distributions of SML and FMI within the sample (Tables 3 and 4). The intra- and interobserver errors were evaluated using intraclass correlation coefficients (ICCs) and Cohen's kappa index. The intra- and interobserver reliabilities for SML and ROI landmarks were very high according to the ICC (means of 0.993 and 0.990, respectively), and Cohen's kappa index for FMI also showed substantial agreement (means of 0.805 and 0.779, respectively).

Based on the GPA and PCA results, PC1 scores were used to construct a multiple regression model for estimation of skeletal maturation. For the female subpopulation, the form-space PC1s of ACV1, ACV2, and ACV3 improved the estima-

Table 3. **Shapiro–Wilk normality test**

	Shapiro–Wilk *W*	*p*-Value
Female		
FMI	0.618	<0.001
SML	0.656	<0.001
Male		
FMI	0.790	<0.001
SML	0.774	<0.001

FMI, Fishman's skeletal-maturation index; SML, Sempé maturation level.

Table 4. **Correlation between Sempé maturation level (SML) and Fishman's skeletal-maturation index (FMI)**

	Female	Male
Pearson's *R* (95%)	0.950	0.956
Spearman's correlation coefficient	0.792	0.897
Kendall's τ	0.692	0.785

Table 5. **Model regions of interest (mROIs) for estimation models and corresponding indicator spaces**

	mROI	Indicator space
Female		
ACV1	Vertebral foramen	Form
ACV2	Posterior arch triangle	Form
ACV3	Vertebral foramen	Form
ACV4	n/a	n/a
Male		
ACV1	n/a	n/a
ACV2	n/a	n/a
ACV3	Vertebral body	Size
ACV4	Vertebral foramen	Size

ACV1, first axial cervical vertebra; ACV2, second axial cervical vertebra; ACV3, third axial cervical vertebra; ACV4, fourth axial cervical vertebra.

tion model relative to the SML simple regression model based on only chronological age. In contrast, in the male subpopulation, only ROI size was significant as a biological indicator. The model ROI (mROI) landmarks are defined in Table 5.

Following the selection of ACV1 vertebral foramen as the first mROI ($mROI_1$), the ACV2 posterior arch triangle and ACV3 vertebral foramen were selected as $mROI_2$ and $mROI_3$, respectively, for the female estimation model. Only the first PC scores of model ROIs were used as predictors to maintain the simplicity of the prediction model while still best representing essential morphological information.

The SML estimation models for the female and male subpopulations were each summarized and compared with the reference model (Table 6). In both models, no shape-related predictor was found to be statistically significant. Rather, in each model, the improvement was imparted by the size of each mROI, the ACV3 vertebral body as $mROI_1$, and the ACV4 vertebral foramen as $mROI_2$.

In the female SML estimation model, R^2 was used as a measure of the extent to which individual variations are explained by chronological age and the forms of the first-to-third ACVs. There was an approximately 8% increase in predictive power compared with the reference model using only chronological age. However, there should be more emphasis on adjusted R^2. In the statistical perspective, a higher adjusted R^2 confirms cross-validity of its corresponding prediction model, demonstrating that the model validity should hold for another sample drawn from the same population. Accordingly, 7.9% enhancement would still be expected to hold for another sample from the same population group. With respect to the adjusted R^2 of the female model, whereas chronological age alone could explain 76.9% of the SML variability, the form-space PC1s of $mROI_1$ to $mROI_3$ explained 84.8%, representing a 7.9% increase in the model's explanatory power overall. For the male estimation model, the adjusted R^2 was above 90%, representing a 1.7% increase relative to the reference model. The 95% PI width average was 285.6 SML units for females and 331.4 SML units for males, equivalent to 1.86 and 2.15 years in chronological age, respectively.

In the female model, the forms of the ACV1 vertebral foramina, ACV2 posterior arch triangle, and ACV3 vertebral foramen changed independently as ossification proceeded. In the male model, ACV3 and ACV4 were seemingly similar, but changed independently over the course of skeletal maturation. These results supported that the extracted forms of ACVs in the female model and their size in the male model were independent of chronological age with respect to SML variability. These estimation models enhanced the predictive power compared with models using chronological age alone. Another significant aspect of these estimation models was the absence of significant multicollinearity between SML predictors in both the female and male models, which was confirmed by multicollinearity tests based on the variance inflation factor (VIF) and the tolerance statistic.

Table 6. **Model regions of interest (mROIs) for estimation models**

	Univariate estimation model				Bivariate estimation model (age + $mROI_i$, i = 1, 2, 3)				Multivariate estimation model (age + $mROI_1$ + $mROI_2$ + $mROI_3$)					
	R^2	Adjusted R^2	Coefficient estimate ± SE	p	R^2	Adjusted R^2	Coefficient estimate ± SE	p	R^2	Adjusted R^2	Coefficient estimate ± SE	p	VIF	1/VIF*
Female														
Age	0.772	0.769	48.08 ± 3.08	<0.001					0.857	0.848	55.72 ± 3.11	<0.001	1.55	0.64
ACV1 model ROI ($mROI_1$)	0.163	0.152	−1.87 ± 0.50	<0.001	0.780	0.774	0.49 ± 0.31	0.113			−0.66 ± 0.32	0.042	2.25	0.45
ACV2 model ROI ($mROI_2$)	0.030	0.017	1.11 ± 0.74	0.137	0.834	0.829	−1.78 ± 0.35	<0.001			−1.67 ± 0.43	<0.001	2.19	0.46
ACV3 model ROI ($mROI_3$)	0.068	0.055	1.99 ± 0.87	0.025	0.825	0.820	−2.07 ± 0.44	<0.001			−1.45 ± 0.49	<0.01	1.99	0.50
Male														
Age	0.886	0.884	70.22 ± 3.76	<0.001					0.907	0.901			1.06	0.94
ACV3 model ROI ($mROI_1$)	0.076	0.056	7.83 ± 4.06	0.060	0.901	0.897	3.52 ± 1.36	0.013			2.62 ± 1.43	0.075	1.19	0.84
ACV4 model ROI ($mROI_2$)	0.001	−0.022	0.26 ± 1.70	0.881	0.900	0.895	1.36 ± 0.55	0.017			0.97 ± 0.57	0.097	1.17	0.86

*Variance inflation factor (VIF) higher than 10 suggests linear relationship between predictors.[43] 1/VIF = the tolerance statistic: values below 0.1 indicate multicollinearity, below 0.2.

Discussion

Our results demonstrated that statistical shape analysis could be used to find specific objects in ACV images. The present study used full GPA and partial GPA to analyze the shape, size, and form of the ROIs of 74 female and 47 male patients. Additionally, a PCA was performed to analyze the between-subject variabilities of these factors. Specifically, the variabilities of the shapes, sizes, and forms were decomposed into orthogonal components, with the first principal component (PC1) explaining the highest variability.

The use of additional PC scores, including successive PC2 scores, would enable the model to contain more information on the shape and form variability of the subject and could enhance the R^2 of a multiple linear regression model. However, to maintain acceptable simplicity in the present prediction model, we used only PC1 scores of shape and form spaces. Thus, in the process of model selection, we chose only indicator variables attaining strong statistical significance.

In the present study, we developed an ACVM method to investigate a biological indicator of skeletal maturation. Our analysis showed the main features of the ACVM method to be the following: 1) minimum subjectivity in ACV image assessment; 2) minimum number of landmarks used but with maximum distinctiveness; 3) valid prediction of skeletal-maturation level using GPA; 4) identification of age-independent biological indicators of skeletal maturation; and 5) identification of intra-independent biological indicators of skeletal maturation. The first two features were based on the methodology, while the third was achieved by constructing a multiple regression model of SML based on mROIs. The last two indicators—age independency and intra-independency—were found among the predictor relationships and were identified while verifying the nonexistence of multicollinearity among the indicators in the model.

The age independency of predictors indicates that the mROIs are independent from chronological age in explaining SML variability. When using conventional lateral images of cervical vertebrae to extract morphometric information that may reflect skeletal-maturation levels, it is intrinsically difficult to obtain statistically significant estimates. The lateral shapes endow vertical dimensionality, which correlates with body height and is thus positively related to chronological age. Therein, the problem of severe multicollinearity arises. But, the ACVM model is unfettered from this issue and can thus improve the reference model based on chronological age. We demonstrated this through a series of tests of tentative ROIs, after which the mROI selections were finalized and applied to the SML estimation model as valid biological indicators.

Our results showed that among female patients, the forms of the ACV1 vertebral foramen, ACV2 posterior arch, and ACV3 vertebral foramen explained the skeletal-maturation level almost independently. Regarding landmark locations and their spatial relationship, the ACV1 proximal curvature and size of the articular surface are embedded in the ACV1 ROI form space. Hence, its form-space PC score conveys information on the form of articular surfaces that adjust their forms to adapt to morphological changes in the cranial base or any functional demands in the region throughout skeletal maturation. The ACV2 posterior arch reflects an increased skeletal mass upon ossification in the craniofacial area. Finally, the ACV3 vertebral foramen provides information on latent factors corresponding to the skeletal-maturation level, other than those reflected in ACV1 and ACV2.

With each ACV almost independently representing SML variations, the portion of SML variation explained by each biological indicator can be understood by the coefficient estimate. The ACV1, ACV2, and ACV3 coefficient absolute values were 0.66, 1.67, and 1.45, respectively, suggesting that the ACV2 posterior arch explains more of the SML variation than ACV1 and ACV3. In the male model, the mROI of ACV3 was weighted with the coefficient estimate of 2.62, which was approximately 2.7 times that of ACV4 (0.97). This implies that ACV3 predominates over ACV4 in its influence on SML, even though the ACV3 vertebral body and ACV4 vertebral

foramen independently explain male SML variation. The mROIs in these estimation models are meaningful, as they substantiate skeletal maturation by responding to it morphologically. The findings of variation in the coefficient estimates among the mROIs of each ACV confirm the differing responses of ACVs to skeletal maturation in females and males.

In cervical vertebrae function, head-nodding movement is performed predominantly through flexion and extension at the atlanto–occipital joint. The atlas articulates with the occipital condyles, and its primary motions are flexion and extension (18, 19). The weight of the head is transferred to the cervical spine through the lateral atlanto-axial articulations of the axis. The superiorly directed odontoid process extending from its body rests within a facet on the atlas that is created by the anterior arch, allowing the atlas and head to rotate from side to side as one unit (19). At the C2-through-C3 junction, the axis body acts as a 'root' within C3, securing the upper cervical spine in the remaining cervical column (18). The articulating surfaces of the inferior and superior intervertebral joints are similar to a saddle joint, maintaining anterior–posterior and medially and laterally directed concavities (20). These functional demands can induce horizontal morphologic changes as skeletal maturation proceeds. This concept is supported by our present study, wherein axial cervical vertebral morphology was utilized and validated as a viable predictor of skeletal-maturation status.

The final female and male SML estimation models and their statistical significances indicate that some latent factors that cause individual discrepancies between somatic growth level and chronological age are morphometrically reflected in ACV and can be captured in the form of PC scores through GPA and PCA. We observed that female skeletal maturation involved more shape-specific ossification, while SML variation in males was indicated by ROI size rather than shapes. Such dimorphism might reflect divergence in the course of ossification between females and males. A more explicit explanation based on the anatomy or physiology of cervical vertebrae is beyond the scope of this study and will require further analysis.

While most previous CVM studies have approached the lateral aspect, here we focused on the axial aspect. Although both aspects are known to be associated with factors such as craniofacial morphology and craniocervical posture (21–24), few studies have investigated axial cervical vertebral structure or function. Therefore, further related studies and three-dimensional CVM, including both lateral and axial aspects, are needed to improve the present method of determining skeletal maturation. Furthermore, as the present study was carried out in a Korean population, additional studies across different ethnicities should be performed to create a further generalized estimation model.

Conclusion

An ACVM method utilizing distinctive anatomical landmarks was confirmed to be useful in explaining individual variability in skeletal maturation. To maintain the objectivity of the axial image acquisition protocol, GPA was used to analyze the simple ACV shape and form rather the full shape. Thus, the ACVM utilizes simple ACV-extracted morphometric information to construct a model to estimate skeletal-maturation status. The simplest morphometric information from ACV provides a statistically significant explanation of the portion of skeletal-maturation variability not dependent on chronological age. Overall, the present results verify ACV as a biological indicator of ossification status and reconfirm the value of ACV as one of few available quantifiers of skeletal maturation.

Clinical relevance

We found that CBCT images were useful for examining the ACV and their morphologic changes. Our results demonstrated that the ACVM method led to improved prediction of skeletal maturation in a Korean population. This

method represents a new way of utilizing readily available CBCT images or medical CT scans taken as part of a patient's clinical evaluation, thus enhancing the cost-effectiveness of CT images. Furthermore, based on the high distinctiveness of landmarks used in the present study, a digitalized evaluation of ACV and automated computation is feasible.

Acknowledgements: This research was supported by a grant from BioMedical Research Institute, Pusan National University Hospital.

References

1. Hagg U, Taranger J. Maturation indicators and the pubertal growth spurt. *Am J Orthod* 1982;82:299–308.
2. O'Reilly M, Yanniello G. Mandibular growth changes and maturation of cervical vertebrae. *Angle Orthod* 1988;58:179–84.
3. Bjork A, Helm S. Prediction of the age of maximum puberal growth in body height. *Angle Orthod* 1967;37:134–43.
4. Hagg U, Taranger J. Menarche and voice changes as indicators of the pubertal growth spurt. *Acta Odontol Scand* 1980;38:179–86.
5. Todd T, Pyle SI. Quantitative study of the vertebral column. *Am J Phys Anthropol* 1928;12:321.
6. Lamparski DG. *Skeletal Age Assessment Utilizing Cervical Vertebrae* [Master's Thesis]. Pittsburgh, PA: Department of Orthodontics, the University of Pittsburgh; 1972.
7. Hassel B, Farman A. Skeletal maturation evaluation using cervical vertebrae. *Am J Orthod Dentofacial Orthop* 1995;107:58–66.
8. Franchi L, Bacetti T, McNamara JA Jr. Mandibular growth as related to cervical vertebral maturation and body height. *Am J Orthod Dentofacial Orthop* 2000;118:335–40.
9. McNamara JA Jr, Brudon WL. *Orthodontics and Dentofacial Orthopedics*. Ann Arbor, MI: Needham Press; 2001. pp. 78–80.
10. Gabriel DB, Southard KA, Qian F, Marshall SD, Franciscus RG, Southard TE. Cervical vertebrae maturation method: poor reproducibility. *Am J Orthod Dentofacial Orthop* 2009;136:478.e1–e7.
11. Chen LL, Xu TM, Jiang JH, Zhang XZ, Lin JX. Quantitative cervical vertebral maturation assessment in adolescents with normal occlusion: a mixed longitudinal study. *Am J Orthod Dentofacial Orthop* 2008;134:720.e1–e7.
12. Chatzigianni A, Halazonetis DJ. Geometric morphometric evaluation of cervical vertebrae shape and its relationship to skeletal maturation. *Am J Orthod Dentofacial Orthop* 2009;136:481.e1–e9.
13. Dryden IL, Mardia KV. *Statistical Shape Analysis*. Chichester: John Wiley & Sons; 1998.
14. Ludlow JB, Davies-Ludlow LE, Brooks SL, Howerton WB. Dosimetry of 3 CBCT devices for oral and maxillofacial radiology: CB Mercury, NewTom 3G, and i-CAT. *Dentomaxillofac Radiol* 2006;35:219–26.
15. Sukovic P. Cone beam computed tomography in craniofacial imaging. *Orthod Craniofac Res* 2003;6:31–6.
16. Sempé M. *La Pédiatrie au Quotidian. Analyse de la Maturation Sequelettique*. Paris: Les Editions INSERM; 1987. Available at: http://www.auxologie.com/mediatheque/pdf/la_pediatrie_au_quotidien.pdf. Accessed February 27, 2013.
17. Bookstein FL. Landmark methods for forms without landmarks: morphometrics of group differences in outline shape. *Med Image Anal* 1997;3:225–43.
18. Bogduk N, Mercer S. Biomechanics of the cervical spine. I: normal kinematics. *Clin Biomech (Bristol, Avon)* 2000;15:633–48.
19. Windle WF. *The Spinal Cord and Its Reaction to Traumatic Injury: Anatomy, Physiology, Pharmacology, Therapeutics*. New York, NY: M Dekker; 1980. p. 384.
20. Penning L, Wilmink JT. Rotation of the cervical spine: a CT study in normal subjects. *Spine* 1987;12:732–8.
21. Huggare J. Association between morphology of the first cervical vertebrae, head posture, and craniofacial structures. *Eur J Orthod* 1991;13:435–40.
22. Hellsing E, Reigo T, McWilliam J, Spangfort E. Cervical and lumbar lordosis and thoracic kyphosis in 8, 11 and 15-year-old children. *Eur J Orthod* 1987;9:129–38.
23. Solow B, Tallgren A. Head posture and craniofacial morphology. *Am J Phys Anthropol* 1976;44:417–35.
24. Sonnensen L, Kjaer I. Cervical column morphology in patients with skeletal class III malocclusion and mandibular overjet. *Am J Orthod Dentofacial Orthop* 2007;132:427.e7–e12.